九州大学学術情報リポジトリ
Kyushu University Institutional Repository

Introduction of a Genetic Algorithm to a Mass-Consistent Model

Harada, Masayoshi
Institute of Tropical Agriculture, Kyushu University

Hayashi, Shizuo
Institute of Tropical Agriculture, Kyushu University

Wakimizu, Kenji
Laboratory or Agricultural Meteorology, Faculty of Agriculture, Kyushu University

https://doi.org/10.5109/24342

出版情報：九州大学大学院農学研究院紀要. 44 (3/4), pp.403-418, 2000-02. Kyushu University
バージョン：
権利関係：

KYUSHU UNIVERSITY

J. Fac. Agr., Kyushu Univ., **44** (3·4), 403–418 (2000)

Introduction of a Genetic Algorithm to a Mass-Consistent Model

Masayoshi Harada, Shizuo Hayashi and Kenji Wakimizu*

Institute of Tropical Agriculture, Kyushu University, 6–10–1 Hakozaki,
Higashi-ku, Fukuoka 812–8581, Japan
(Received October 29, 1999 and accepted November 5, 1999)

In this paper, Gaussian precision moduli (weights) included in the mass-consistent model, which is one of numerical simulations predicting the three-dimensional wind fields based on the wind measurements, was examined. In the mass-consistent model, reasonable wind fields are calculated by adjusting the first estimated values interpolated from several observed results to satisfy mass conservation utilizing the calculus of variation. Gaussian precision moduli decide distributions of modifications for each component of wind velocities, and directly affect the calculated results. Optimal values of these coefficients were estimated by using a genetic algorithm so as to minimize the deviation between the observed values and the calculated results. As a result, the ratio of weights in the horizontal components was affected by the direction of the eminent wind, regardless of the same condition for the stability of atmosphere.

In conclusion, the mass-consistent model produced a valid result in that the relation between the underlying topography and wind field features was sufficiently represented by introducing the genetic algorithm.

INTRODUCTION

It is essential to grasp a three-dimensional wind field in a complex terrain in regional meteorological problems, such as the dispersion of air pollution in coastal and hilly regions, and the founding of an optimum wind energy site for the deployment of wind turbines. However, observations at single points alone are not suitable to represent the complex wind field because the atmospheric airflow is significantly affected by the underlying topography. Therefore, model simulation plays an important role to produce the three-dimensional description of wind field characteristics that cannot be obtained by extensive field measurements.

Dickerson (1978) calculated the wind field with a two-dimensional mass-conservative flux (MASCON) model to simulate the air quality of the Sun Francisco Bay Area. Sherman (1978) developed the mass-adjusted three-dimensional wind field (MATHEW) model to provide a pollutant transport model. The numerical model that calculates the mean wind field satisfying the continuity equation within the volume specified is called the mass-consistent model, and has been applied to compute the spatial distribution of wind speeds and their variation with height. Gross (1995) examined the applicability of the mass-consistent wind model for different numbers of input wind data by utilizing a three-dimensional nonhydrostatic model. Castino and Tombroul (1998) introduced simple parameterizations of the internal boundary layer concept in the mass consistent

* Laboratory of Agricultural Meteorology, Faculty of Agriculture, Kyushu University, 6–10–1 Hakozaki, Higashi-ku, Fukuoka 812–8581, Japan

model, showing the satisfactory model improvement.

The mass-consistent model is a numerical simulation method that the wind field interpolated from observed values of wind speeds and wind directions, and then modified by the calculus of variation under the constraint of the continuity equation. Therefore, this is different from a numerical simulation of fluid flow in a strict sense. Although the mass-consistent model is a relatively simple physical model, the modeled field has been judged to give a rather satisfactory description of winds (Zhang and Shuto, 1990; Ishikawa, 1994; Abdeladim *et al.*, 1996; Gallino *et al.*, 1998; Finardi *et al.*, 1998).

The purpose of this paper is to introduce a basic algorithm of the mass-consistent model and show the application to the three-dimensional wind field of Waita mountain. This model contains three important weights concerned with the stability of atmosphere, with the appropriateness of the final wind field depending on the specification of these parameters. These parameters are given by empirical assumption or by trial-and-error, and quantitative appraisement has not been established. We then utilize the genetic algorithm to search optimal values of weights that have an effect on the accuracy of the mass-consistent model.

MASS CONSISTENT MODEL

The mass-consistent model reconstructs a three-dimensional wind field starting from several horizontal wind speeds and direction measurements near the earth's surface through a two-step procedure. First, the observed wind field data is interpolated and extrapolated on to numerical grid points defined within an objective area. Next, reliable three-dimensional wind fields are predicted from the first estimated values by the calculus of variation so that adjusted velocity components satisfy mass conservation.

First Estimated Values of Wind Fields

In the general method, interpolated velocity values on grid points are calculated by the weighted mean using the reciprocal number of squared distance between the aimed grid point and each measuring point;

$$\left.\begin{aligned} U_{i,j} &= \sum_k W_{i,j,k}\, U_k \Big/ \sum_k W_{i,j,k} \\ W_{i,j,k} &= 1 / r_{i,j,k}{}^2 \end{aligned}\right\} \tag{1}$$

where $U_{i,j}$ is the interpolated wind velocity on the grid point (i, j), U_k is the wind velocity on the measuring point k, $r_{i,j,k}$ is the distance between the grid point and the measuring point and $W_{i,j,k}$ is the weight. Since it is difficult to observationally acquire detailed vertical profiles of wind speeds and directions, we calculated first estimated values on grid points in the horizontal plane located at the height of wind measurement z_s from equation (1), and then estimated vertical profiles of wind velocities based on these interpolated values.

This paper treats the three-dimensional wind fields within the atmospheric boundary layer which consists of the surface boundary layer and the Ekman layer. Vertical wind profiles were determined in each layer. In the surface boundary layer, the vertical profile

of wind speed obeys the logarithmic law;

$$U(z) = \frac{u_*}{\kappa} \ln\left(\frac{z}{z_o}\right), \qquad z \le h_s \tag{2}$$

where z is the height, u_* is the friction velocity, κ is the Von Kármán constant (=0.4), z_o is the roughness length, and h_s denotes thickness of the surface boundary layer. Generally, the value of z_o in a forest area seems to take 1.0 m. If z_s is the height of the measuring point and u_s denotes the wind speed at z_s, the equation (2) then becomes

$$U(z) = \frac{\ln(z/z_o)}{\ln(z_s/z_o)} u_s, \qquad z \le h_s. \tag{3}$$

On the other hand, the vertical profile of horizontal wind velocities in the Ekman layer can be represented as the Ekman spiral in such cases where the turbulent diffusion coefficient is constant. Yet, we need to acquire information such as the geostrophic wind and diffusion coefficient to prescribe this profile, and these complicate the process of wind velocity calculation. Therefore, to facilitate calculations, this paper utilizes a power law;

$$U(z) = u_e\left(\frac{z}{z_e}\right)^p, \qquad h_s < z < h_e \tag{4}$$

where u_e and z_e are the horizontal wind velocity and the height of upper edge of the surface boundary layer respectively, and h_e denotes thickness of the atmospheric boundary layer. In this paper, the exponent p is set to 0.2 as a typical value in the general land area.

Correction of Wind Fields by the Calculus of Variation

Generally, in the first step the vertical component of mean wind velocity cannot be obtained due to a restriction of the wind observation method. More so, the first estimated velocity distribution obtained by equation (1) does not satisfy any physical conservation relation, as well as not considering the impact of the terrain surface. In the second step, reliable three-dimensional mass conservative wind fields are estimated from the first estimated values by the calculus of variation so that adjusted velocity components satisfy mass conservation. That is, under the constraint of the continuity equation;

$$\frac{\partial u}{\partial x} + \frac{\partial v}{\partial y} + \frac{\partial w}{\partial z} = 0 \tag{5}$$

where x, y are the horizontal direction, z is the vertical direction, and u, v and w are respectively the adjusted velocity components in the x, y and z directions, we think the variational problem can minimize the summation of modification between adjusted and interpolated values;

$$E[u, v, w] = \int_V \left\{ \alpha_u^2 (u - u_0)^2 + \alpha_v^2 (v - v_0)^2 + \alpha_w^2 (w - w_0)^2 \right\} dV \tag{6}$$

where u_0, v_0 and w_0 are interpolated values, V denotes the volume integral and α_u^2, α_v^2 and α_w^2 are the Guassian precision moduli in the horizontal and vertical directions. The

details for these coefficients will be described later. By introducing the Lagrange multiplier λ, the functional used in this model is given as follows,

$$E[u,v,w,\lambda]=\int_V \left\{ \alpha_u^2(u-u_0)^2+\alpha_v^2(v-v_0)^2+\alpha_w^2(w-w_0)^2 + \lambda\left(\frac{\partial u}{\partial x}+\frac{\partial v}{\partial y}+\frac{\partial w}{\partial z}\right)\right\} \mathrm{d}V . \tag{7}$$

The stationary condition for the variational problem of equation (7) is given as the following;

$$\begin{aligned}\delta E[u,v,w,\lambda]=&\int_V \left(2\alpha_u^2(u-u_0)-\frac{\partial\lambda}{\partial x}\right)\delta u+\left(2\alpha_v^2(v-v_0)-\frac{\partial\lambda}{\partial y}\right)\delta v \\ &+\left(2\alpha_w^2(w-w_0)-\frac{\partial\lambda}{\partial z}\right)\delta w+\left(\frac{\partial u}{\partial x}+\frac{\partial v}{\partial y}+\frac{\partial w}{\partial z}\right)\delta\lambda\Big\}\,\mathrm{d}V \\ &+\int_S \lambda n_x\delta u\,\mathrm{d}y\,\mathrm{d}z+\int_S \lambda n_y\delta v\,\mathrm{d}z\,\mathrm{d}x+\int_S \lambda n_z\delta w\,\mathrm{d}x\,\mathrm{d}y=0\end{aligned} \tag{8}$$

where n_x, n_y and z_z are the outward positive unit normal vectors in the x, y and z directions respectively, and S denotes the surface integral. Since this equation is identically applicable to arbitrary variations δu, δv, δw and $\delta\lambda$, the associated Euler–Lagrange equations whose solution minimizes equation (7) are

$$u=u_0+\frac{1}{2\alpha_u^2}\frac{\partial\lambda}{\partial x} \tag{9}$$

$$v=v_0+\frac{1}{2\alpha_v^2}\frac{\partial\lambda}{\partial y} \tag{10}$$

$$w=w_0+\frac{1}{2\alpha_w^2}\frac{\partial\lambda}{\partial z} \tag{11}$$

$$\frac{\partial u}{\partial x}+\frac{\partial v}{\partial y}+\frac{\partial w}{\partial z}=0 \tag{12}$$

and the boundary conditions are

$$\left.\begin{aligned}&\lambda n_x\delta u=0, \quad (x\text{-direction})\\ &\lambda n_y\delta v=0, \quad (y\text{-direction})\\ &\lambda n_z\delta w=0, \quad (z\text{-direction})\end{aligned}\right\}. \tag{13}$$

To easily apply the mass-consistent model to the arbitrary terrain, the partial differential equations and boundary conditions can be dealt with in the coordinate system along the ground surface;

$$\xi=x, \quad \eta=y, \quad \zeta=z-h(x,y) \tag{14}$$

where $h(x, y)$ is the surface topography height. Hereby, equations of (9) to (12) are transformed into

$$u = u_0 + \frac{1}{2\alpha_u^2}\frac{\partial \lambda}{\partial \xi} - \frac{1}{2\alpha_u^2}\frac{\partial h}{\partial \xi}\frac{\partial \lambda}{\partial \zeta} \tag{15}$$

$$v = v_0 + \frac{1}{2\alpha_v^2}\frac{\partial \lambda}{\partial \eta} - \frac{1}{2\alpha_v^2}\frac{\partial h}{\partial \eta}\frac{\partial \lambda}{\partial \zeta} \tag{16}$$

$$w = w_0 + \frac{1}{2\alpha_w^2}\frac{\partial \lambda}{\partial \zeta} \tag{17}$$

$$\frac{\partial u}{\partial \xi} + \frac{\partial v}{\partial \eta} + \frac{\partial w}{\partial \zeta} - \frac{\partial h}{\partial \xi}\frac{\partial u}{\partial \zeta} - \frac{\partial h}{\partial \eta}\frac{\partial v}{\partial \zeta} = 0, \tag{18}$$

and the boundary conditions of (11) become to

$$\left.\begin{aligned} &\lambda n_\xi \delta u = 0, \quad (\xi - \text{direction}) \\ &\lambda n_\eta \delta v = 0, \quad (\eta - \text{direction}) \\ &\lambda n_\zeta \left(\delta w - \frac{\partial h}{\partial \xi}\delta u - \frac{\partial h}{\partial \eta}\delta v \right) = 0, \quad (\zeta - \text{direction}) \end{aligned}\right\}. \tag{19}$$

Two types of boundary conditions can be considered from equation (19). One is

$$\lambda = 0 \tag{20}$$

which means that an adjustment of the velocity component parallel to the boundary is zero. In general, the normal derivative of λ is not zero when λ is zero on a boundary. A non-zero adjustment of the velocity component normal to the boundary implies a change in the amount of mass entering or leaving the volume. Therefore, the boundary condition of $\lambda = 0$ is appropriate for open or flow-through boundary. Another instance is under the condition in which the variation of the normal velocity component is zero on boundary;

$$n_\xi \delta u = 0, \quad (\xi - \text{direction}) \tag{21}$$

$$n_\eta \delta v = 0, \quad (\eta - \text{direction}) \tag{22}$$

$$n_\zeta \left(\delta w - \frac{\partial h}{\partial \xi}\delta u - \frac{\partial h}{\partial \eta}\delta v \right) = 0, \quad (\zeta - \text{direction}). \tag{23}$$

In this case, the adjusted value of the normal velocity must be the observed value on that boundary. If the observed normal velocity is zero, the boundary condition will imply no transport of mass across the boundary. Therefore, this condition is used for closed, or no-flow-through boundary. In this paper, it was assumed that the boundary condition of equation (23) was established on the ground surface, and the equation (20) was utilized for other boundaries.

The partial differential equation for λ is derived by differentiating equations of (15) to (17) and substituting the results into (18);

$$\begin{aligned} &\frac{1}{2\alpha_u^2}\frac{\partial^2 \lambda}{\partial \xi^2} + \frac{1}{2\alpha_v^2}\frac{\partial^2 \lambda}{\partial \eta^2} + \left\{ \frac{1}{2\alpha_u^2}\left(\frac{\partial h}{\partial \xi}\right)^2 + \frac{1}{2\alpha_v^2}\left(\frac{\partial h}{\partial \eta}\right)^2 \right\}\frac{\partial^2 \lambda}{\partial \zeta^2} - \frac{1}{\alpha_u^2}\frac{\partial h}{\partial \xi}\frac{\partial^2 \lambda}{\partial \xi \partial \zeta} \\ &\quad - \frac{1}{\alpha_v^2}\frac{\partial h}{\partial \eta}\frac{\partial^2 \lambda}{\partial \eta \partial \zeta} - \left(\frac{1}{2\alpha_u^2}\frac{\partial^2 h}{\partial \xi^2} + \frac{1}{2\alpha_v^2}\frac{\partial^2 h}{\partial \eta^2} \right)\frac{\partial \lambda}{\partial \zeta} + \frac{\partial u_0}{\partial \xi} + \frac{\partial v_0}{\partial \eta} + \frac{\partial w_0}{\partial \zeta} \\ &\quad - \frac{\partial h}{\partial \xi}\frac{\partial u_0}{\partial \zeta} - \frac{\partial h}{\partial \eta}\frac{\partial v_0}{\partial \zeta} = 0. \end{aligned} \tag{24}$$

In consideration of the equation (23), the equation for λ on the ground surface is given as follows,

$$\frac{1}{\alpha_u^2}\frac{\partial h}{\partial \xi}\frac{\partial \lambda}{\partial \xi}+\frac{1}{\alpha_v^2}\frac{\partial h}{\partial \eta}\frac{\partial \lambda}{\partial \eta}-\left(\frac{1}{2\,\alpha_w^2}+\frac{1}{\alpha_u^2}\left(\frac{\partial h}{\partial \xi}\right)^2+\frac{1}{\alpha_v^2}\left(\frac{\partial h}{\partial \eta}\right)^2\right)\frac{\partial \lambda}{\partial \zeta}$$
$$+\frac{\partial h}{\partial \xi}u_0+\frac{\partial h}{\partial \eta}v_0-w_0=0\,. \tag{25}$$

Equations approximating (24) and (25) by the finite difference are solved for λ using successive over relaxation (SOR), and second estimated velocity components u, v and w are calculated from equations of (15) to (17).

ESTIMATION OF WEIGHTS BY GENETIC ALGORITHM

Guassian Precision Moduli

Parameters α_u^2, α_v^2 and α_w^2 are weights which represent the distributions of modifications of the horizontal and the vertical component, depending on the stability of atmosphere. That is, the weights can be changed according to the state of the atmospheric boundary layer when measuring wind speeds and directions. The final wind field simulated by the mass-consistent model is sensitive to how to choose α_u^2, α_v^2 and α_w^2. Guassian precision moduli $\alpha_i^2(i=u, v, w)$ can be defined as follows,

$$\alpha_i^2=\frac{1}{2}\sigma_i^{-2} \qquad (i=u, v, w) \tag{26}$$

where $\sigma_i^2(i=u, v, w)$ denotes deviation of the observed field from the desired adjusted field.

Generally, on the assumption of $\alpha_u^2=\alpha_v^2$, the value of α_u^2/α_w^2 has been discussed on the basis of comparing orders of horizontal and vertical components of wind velocities due to the fact that $(\alpha_u/\alpha_w)^2\equiv(\sigma_w/\sigma_u)^2$ seems to be proportional to the magnitude of the expected $(w/u)^2$. If this ratio is larger, the adjustment is predominantly in the vertical component. If it is smaller, the horizontal adjustment dominates. Dickerson (1978) acquired reasonable horizontal and vertical adjusted fluxes by supposing that $(\alpha_u/\alpha_w)^2$ was 10^9. Also, Sharman (1978) assumed that the value of $(\sigma_w/\sigma_u)^2$ was approximately 10^{-4}, the values of α_u^2 and α_w^2 were taken to be 0.5 and 5000, respectively. Furthermore, Zhang and Shuto (1990) established the ratio Gaussian precision moduli, $\alpha\ (=\alpha_u/\alpha_w)$, so that it was equal to the ratio σ_w/σ_u, and could obtain the optimum value of $\alpha=0.13$. However, there is need for clarification in that α_u^2 and α_w^2 were simply determined by empirically comparing orders of the horizontal and the vertical velocity component. More so, we think that the assumption of $\alpha_u^2=\alpha_v^2$ is not always valid because this needs to be taken into consideration the feature of topography and the stability of atmosphere have influence on not only the ratio of the weight of the horizontal component and one of the vertical component, but also the ratio of weights in the W–E–direction, and in the S–N–direction.

In this paper, Gaussian precision moduli α_u^2, α_v^2 and α_w^2 are estimated by a genetic algorithm in order to minimize the deviation between measured wind speed and calculated results obtained by the mass–consistent model. We think that it is beneficial to

find out optimal values of α_u^2, α_v^2 and α_w^2 for relating Gaussian precision moduli to atmospheric conditions when measuring wind speeds and directions.

Genetic Algorithm

A genetic algorithm (GA) is an optimization technique using artificial processes patterned on natural selection, evolution, and the principle of survival of the fittest. An important characteristic of this algorithm is the coding of the variables that describe the optimization problem. The variables are transformed into a binary string of specific length with each string being called a chromosome. If the problem has more than one variable, a multivariable coding is constructed by concatenating as many single variable codings as the number of the variables in the problem. Individuals in the population are evaluated quantitatively by applying an objective function (phenotype) on the solution encoded by their chromosomal representation, and then fitness of each individual, which indicates the worth of the solution to the problem, is calculated depending on the method suitably set by a GA modeler. It is a necessary for the GA to define the phenotype and to estimate the fitness.

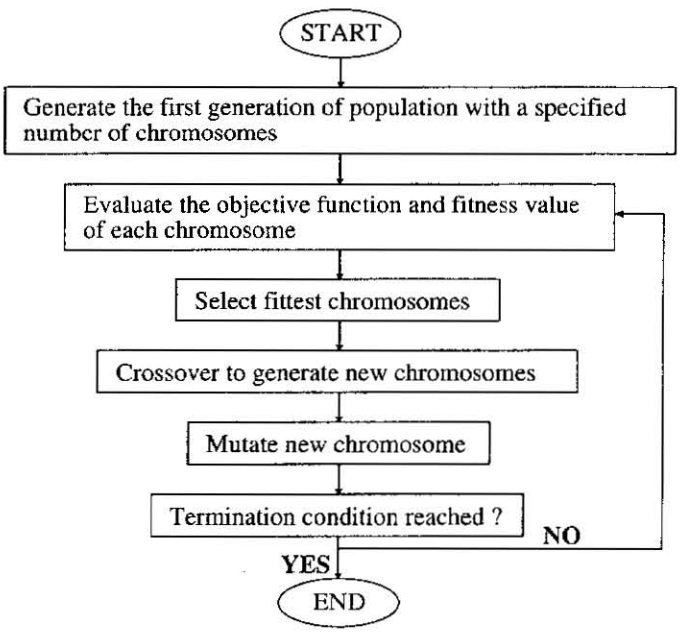

Fig. 1. Flowchart of genetic algorithm.

Fig. 1 shows the basic outline of the GA that starts with creation of an initial population using a random number. From the current population, the next generation evolves by performing three distinct operations, namely, reproduction (selection and multiplication), crossover, and mutation. First, the next generation is then reproduced

based on the statistic of this population by following the weighted roulette wheel method, which then follows a bias law that assigns probabilities to the members of the population analogous to the statistics of the generation. In this way, the next generation evolves where the fittest have survived and increased their presence, while individuals having lower fitness die out or disappear from the generation. Furthermore, the individuals having the maximum fitness, so-called elite, are invariably passed to the next generation. Secondly, with a specified probability of crossover (crossover rate), two members of the population are then selected randomly and modified by exchanging the right part of their string at a randomly selected position. This is referred to as a single-point crossover scheme. The crossover rate determines whether or not a crossover will be applied to the selected pair of parents. Finally, the mutation operation is performed by randomly changing the values of certain genes. In normal mutation, each bit corresponding to the gene composing of the individual is altered as zero to one, or one to zero based on a probability of mutation (mutation rate). The GA evolves the population of chromosomes over many generations until a terminating criterion is met.

The GA works with a collection of solutions, while the search space is explored in a highly parallel and efficient manner through crossover and mutation. Since the GA is superior in that it is less likely to get trapped in regions containing local minima and can perform a global search of the search space, the GA has been applied to various fields (Liong *et al.* (1995) and Mohan (1997)).

Definition of Genotype and Phenotype

The search problem which becomes the object in this study is to estimate optimal values of α_v^2 and α_w^2, which minimize the error between observed values and calculated results, under the condition of $\alpha_u^2=1$. A coded string consists of 2 coded substrings each of 8 binary bits, which provides a resolution of 25 points to cover the range of each weighted coefficient in the mass-consistent model used. The string of each gene corresponds to the Guassian precision moduli α_v^2 and α_w^2 by the following equations;

$$N_1=2^7B_1+2^6B_2+2^5B_3+2^4B_4+2^3B_5+2^2B_6+2^1B_7+2^0B_8+1 \tag{27}$$

$$N_2=2^7B_9+2^6B_{10}+2^5B_{11}+2^4B_{12}+2^3B_{13}+2^2B_{14}+2^1B_{15}+2^0B_{16}+1 \tag{28}$$

$$\alpha_v^2=\frac{b_v-a_v}{255}(N_1-1)+a_v \tag{29}$$

$$\alpha_w^2=\exp\left\{\frac{\log b_w-\log a_w}{255}(N_2-1)+\log a_w\right\} \tag{30}$$

where $B_i(i=1, 2, \cdots, 16)$ is the value of gene which takes zero or one, a_v and b_v denote the lower limit and upper limit of the range of α_v^2 respectively, and a_w and b_w denote the lower limit and upper limit of the range of α_w^2 respectively. Since it is considered that the order of wind velocity component u is similar to one of v, both the values of a_v and b_v were set to 0.5 and 1.5. On the other hand, considering the observations in past studies and the ratio of order in the horizontal and the vertical wind velocity component, the values of a_w and b_w were set to 10^1 and 10^4, respectively. The method for estimating the fitness will be described later.

RESULTS AND DISCUSSION

Calculated Region and Conditions

The calculated region was a 2 km×2 km hilly area where the Waita mountain (about 1500 m above sea level) is located in the center, as shown in Fig. 2. In numerical simulations, a grid resolution of 100 m was used, leading to 21 horizontal grid points. It was assumed that the distance from ground surface to upper edge in the atmospheric boundary layer h_c and thickness of the surface boundary layer h_s were both 1000 m and 100 m respectively, and that vertical mesh interval was 20 m.

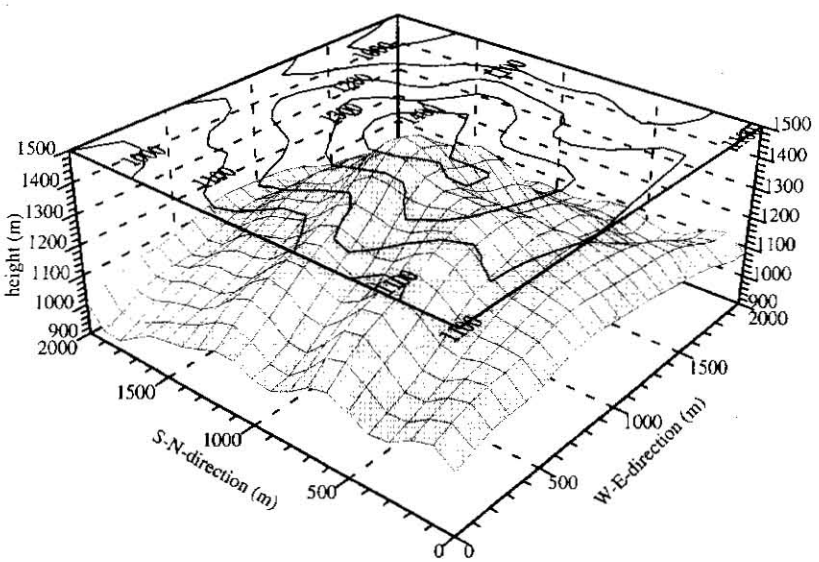

Fig. 2. Three-dimensional perspective view and contours of the hilly simulation area.

The input observational data for wind speeds and directions was calculated based on the experimental values obtained from a vector rain gauge by Sakanoue (1969). For details concerning the estimation process of the wind speed and direction from precipitation obtained with the vector rain gauge, the reader should refer to the paper written by Wakimizu *et al.* (1988). The numerical simulations by the mass-consistent model were performed for the two cases, and the computational conditions for wind speeds and directions is summarized in Table 1, in which wind directions of north, east, south and west are 0°, 90°, 180° and 270°, respectively.

The stability of atmosphere in each case was estimated utilizing the Richardson number,

$$R_i = \frac{g}{T} \cdot \frac{\mathrm{d}\Theta/\mathrm{d}z}{(\mathrm{d}U/\mathrm{d}z)^2} \approx (z_1 \cdot z_2)^{1/2} \cdot \frac{g}{T} \cdot \ln(z_1/z_2) \frac{\Theta_1 - \Theta_2}{(U_1 - U_2)^2} \tag{31}$$

Table 1. Observed values for the wind speeds and directions obtained by the vector rain gauge.

Coordinate (ξ, η)	case 1		case 2	
	speed (m/s)	direction (°)	speed (m/s)	direction (°)
A (1210, 1000)	9.431	268.4	9.327	174.5
B (820, 1000)	10.160	188.9	4.126	184.2
C (1000, 820)	7.767	196.1	9.787	104.8
D (1000, 1230)	8.037	253.2	3.189	98.3
E (1540, 1000)	7.125	200.1	4.991	101.3
F (220, 1000)	9.337	184.0	6.603	97.3
G (1000, 1000)	9.734	265.9	7.542	109.7

where T is the temperature, g is the gravitational acceleration, Θ is the potential temperature of air, and U is the mean wind velocity. Since there was no observed result by AMeDAS for a circumference for Waita mountain, we substituted the upper layer data obtained at the Fukuoka district meteorological observatory. As a result, the Richardson numbers in case 1 and case 2 were 3.55 and 2.96, respectively.

Optimum Value of Gaussian Precision Moduli

To examine the validity of results simulated by the mass-consistent model, we calculated the mean square error between the observed and calculated wind velocities;

$$\left.\begin{aligned} U_{rms}^2 &= \sum_{i=1}^{M} \left(U_{o,i} - U_{c,i}\right)^2 / M \\ u_{rms}^2 &= \sum_{i=1}^{M} \left(u_{o,i} - u_{c,i}\right)^2 / M \\ v_{rms}^2 &= \sum_{i=1}^{M} \left(v_{o,i} - v_{c,i}\right)^2 / M \end{aligned}\right\} \tag{32}$$

where subscripts o and c represent observed and calculated values respectively, M is the number of measuring points, u and v are both wind velocity components in the W-E-direction and the S-N-direction, and $U=\sqrt{u^2+v^2}$. Table 2 and Table 3 show variations of root mean square errors , U_{rms}, u_{rms} and v_{rms}, and the products of u_{rms} and v_{rms} when varying values of the weight α_u^2 operate under the condition $\alpha_v^2=1.0$, and when varying α_v^2 operates under the condition of $\alpha_u^2=10^2$, respectively. It can be seen from Table 2 that mean square error between the observed values and the calculated results decrease with a decrease of α_u^2 in the case of fixing values of α_v^2. Table 3 indicates the tendency such that with an increase of α_v^2, values of U_{rms} and u_{rms} increases, while one of v_{rms} decrease. Also, it is found from Table 3 that the mean square error of wind speed $U(=\sqrt{u^2+v^2})$ in case 1 is the smallest at $\alpha_v^2=0.6$ when fixing the value of α_u^2 as 10^2. However, the accuracy of this calculated result in this case is low for the wind direction because the mean square error of the velocity component in the S-N direction is relatively large. Therefore, the using of U_{rms} is not suitable for the calculation of fitness in the GA. In this paper, to relatively estimate the accuracy of numerical simulations in considering the wind direction as well as the wind velocity, the reciprocal number of the

Table 2. Variations of root mean square error with α_v^2 under the condition of α_w^2=1.0

α_v^2	case 1				case 2			
	U_{rms} (m/s)	u_{rms} (m/s)	v_{rms} (m/s)	$u_{rms} \cdot v_{rms}$ (m^2/s^2)	U_{rms} (m/s)	u_{rms} (m/s)	v_{rms} (m/s)	$u_{rms} \cdot v_{rms}$ (m^2/s^2)
10^1	1.625	1.551	1.939	3.007	3.918	3.975	2.088	8.300
10^0	1.616	1.484	1.906	2.829	3.559	3.646	2.047	7.463
10^{-1}	1.571	1.292	1.814	2.344	2.665	2.817	1.921	5.411
10^{-2}	1.482	1.152	1.904	2.193	2.653	2.890	1.597	4.615

Table 3. Variations of root mean square error with α_v^2 under the condition of α_w^2=10^{-2}

α_v^2	case 1				case 2			
	U_{rms} (m/s)	u_{rms} (m/s)	v_{rms} (m/s)	$u_{rms} \cdot v_{rms}$ (m^2/s^2)	U_{rms} (m/s)	u_{rms} (m/s)	v_{rms} (m/s)	$u_{rms} \cdot v_{rms}$ (m^2/s^2)
0.6	1.467	1.201	1.867	2.242	2.403	2.329	2.488	5.795
0.8	1.489	1.223	1.824	2.231	2.530	2.599	2.178	5.661
1.2	1.703	1.346	1.647	2.217	2.719	2.935	1.697	4.981
1.4	1.932	1.617	1.633	2.641	3.176	2.637	2.619	6.906

product of u_{rms} and v_{rms} was utilized as the fitness.

Table 4 shows the optimal values of α_v^2 and α_m^2 obtained by the GA. As for the weight of the vertical wind velocity component, the value of case 1 was nearly equal to the one of case 2, and is considered that this result was attributable to the stability of atmosphere. For example, the Richardson number of case 1 and case 2 were almost the same. On the other hand, with reference to the weight of the velocity component in the S–N–direction, there was the remarkable difference between case 1 and case 2 regardless of the same atmospheric conditions. It is assumed that such a result was reflected by an influence of the terrain on the wind fields, and differed the direction of the eminent wind.

Table 4. Optimal values of α_v^2 and α_m^2 estimated by the GA

	α_v^2	α_m^2	U_{rms} (m/s)	u_{rms} (m/s)	v_{rms} (m/s)	$u_{rms} \cdot v_{rms}$ (m^2/s^2)
case 1	0.696	53.025	1.437	1.167	1.826	2.131
case 2	1.145	52.406	2.662	2.866	1.687	4.835

Horizontal and Vertical Wind Vectors

Fig. 3 and Fig. 4 show variations of horizontal wind vectors, in which heights above sea level are shown for every 100 m, simulated by the mass–consistent model with heights

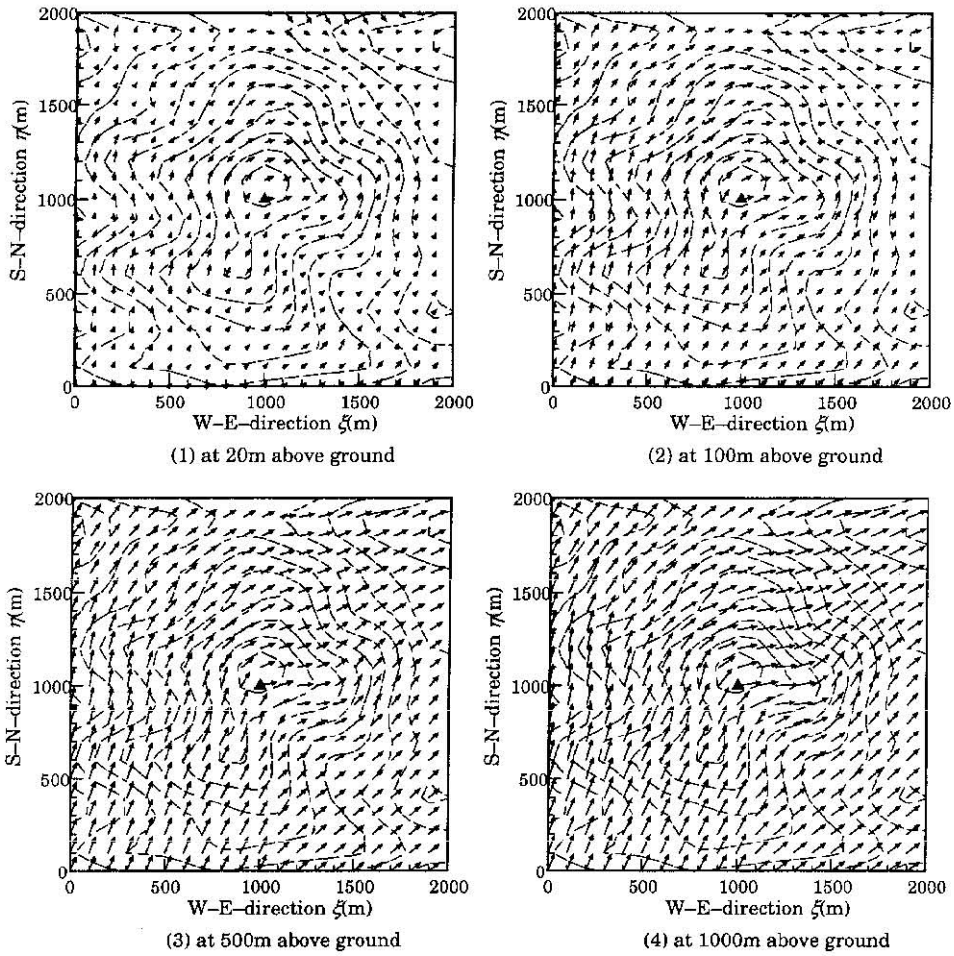

Fig. 3. Horizontal wind vectors in case 1.

in case 1 and case 2. It is found from Fig. 3 that there are differences of wind directions around the ground and at the upper layer of the atmosphere in the x=1000～1500 m and y=1600～2000 m region, and in the x=1400～1600 m and y=700～1500 m region. That is, airflow along the terrain appears clearly in the region of $\zeta \leq 100$ m. Meteorological phenomena like this can be seen in case 2.

Fig. 5 shows variations of wind vectors in the $\xi - \zeta$ section, in which the components in the vertical direction are represented twenty times larger than those in the horizontal direction in order to emphasize the vertical wind velocity components, with coordinates in the S–N–direction. Fig. 6 shows variations of distributions of vertical velocities with heights in case 1. It is found from Fig. 5 that the airflow rose and descended according to

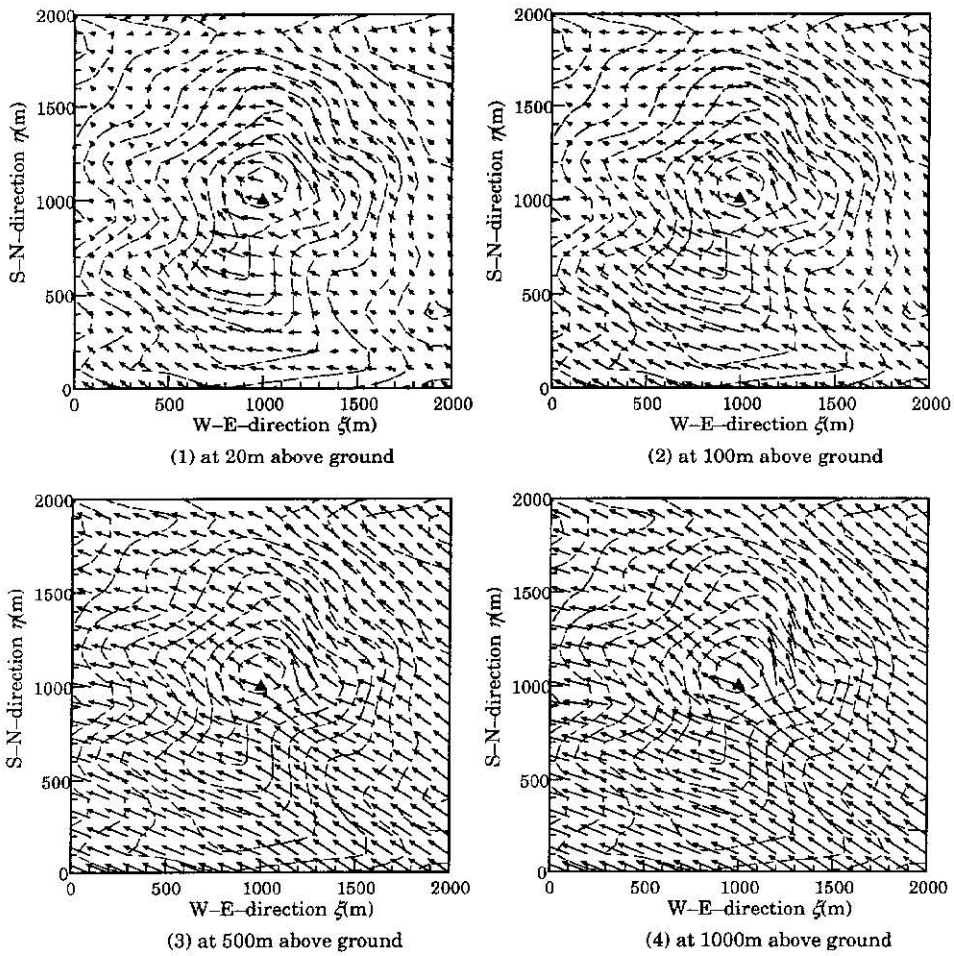

Fig. 4. Horizontal wind vectors in case 2.

the terrain gradient in the surface boundary layer, and that the wind velocity components became less in the vertical direction and zero in the upper layer. It is found from Fig. 6 that vertical wind velocities around the ground surface were intricately distributed due to the effect of the ground gradient on the wind field. Also, distributions of the rising flow and the descending flow in the lower layer ($\zeta \leq 100$ m) were clear, for example strong rising and descending flows were generated in the x=600～800 m and y=300～500 m region and in the x=1200～1600 m and y=1100～1500 m region respectively, while values of the vertical component of wind velocities were nearly zero in the upper layer ($\zeta \geq$ 500 m).

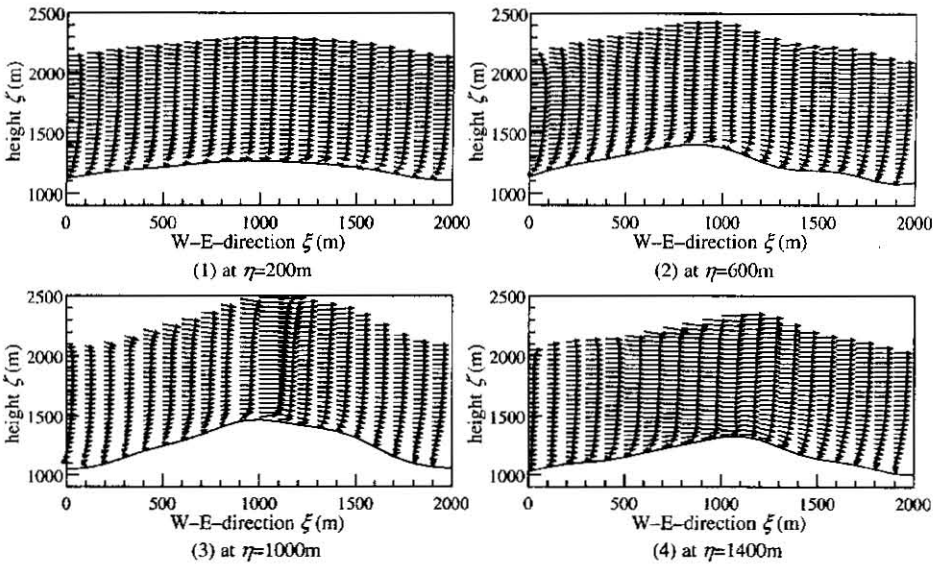

Fig. 5. Wind vectors in the $\xi - \zeta$ section (case 1).

CONCLUSIONS

In this study, numerical simulations of the three-dimensional wind fields in the circumference of Waita mountain were performed by using the mass-consistent model and optimal values of the Gaussian precision moduli, which have an effect on the calculated results, were estimated by genetic algorithm. As a result, both two cases chosen as the subject of the study had the same stability of atmosphere as well as similar weights in the vertical component. More so, for the ratio of the weight in the W-E component and the S-N component, there was a remarkable difference between two cases, such a result seeming to be attributed to the difference of the effects from the terrain gradients on wind fields by directions of the eminent wind. In conclusion, the introduction of the genetic algorithm to the mass-consistent model is valid, and wind vectors simulated by this method represent sufficiently the relation between the underlying topography and wind field features.

REFERENCES

Abdeladim, K., R. Romeo and S. Magri 1996 Wind mapping of a region in the north-east of Algeria, *Renewable Energy*, **9**(1–4): 789–793

Castino, F. and M. Tombrou 1998 Parameterization of convective and stable internal boundary layers into mass consistent models, *Journal of Wind Engineering and Industrial Aerodynamics*, **74–6**: 239–247

Dickerson, M. H. 1978 MASCON – A Mass Consistent Atmospheric Flux Model for Regions with Complex Terrain, *Journal of Applied Meteorology*, **17**: 241–253

Finardi, S., G. Tinarelli, P. Faggian and G. Brusasca 1998 Evaluation of different wind field modeling

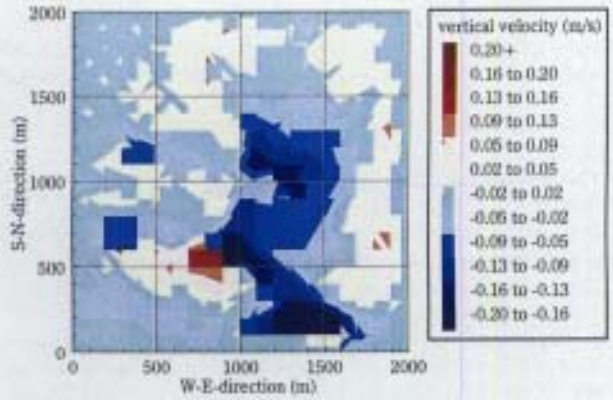

(1) at 20m above ground

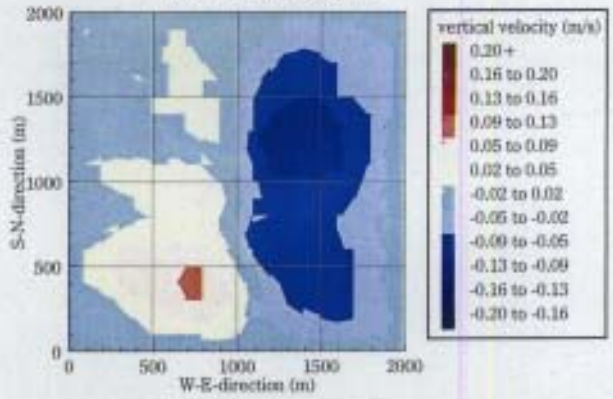

(2) at 100m above ground

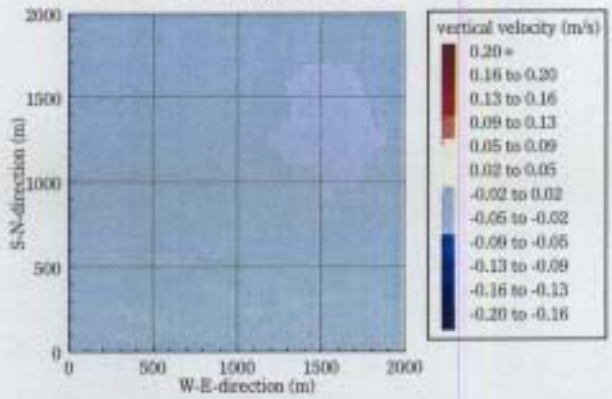

Fig. 6. Contours of vertical wind velocities in case 1.

techniques for wind energy applications over complex topography, *Journal of Wind Engineering and Industrial Aerodynamics*, **74**–6: 283–294

Gallino, S., A. Mazzino and C. F. Ratto 1998 A simple procedure to account for non–kinematic effects in a mass–consistent wind model, *Journal of Wind Engineering and Industrial Aerodynamics*, **74**–6: 229–237

Gross, G 1996 On the applicability of numerical mass–consistent wind field models, *Boundary–Layer Meteorology*, **77**(3–4): 379–394

Ishikawa, H. 1994 Mass–Consistent Wind Model as a Meteorological Preprocessor for Tracer Transport Models, *Journal of Applied Meteorology*, **33**: 733 743

Liong, S. Y., W. T. Chan and J. ShreeRam 1995 Peak–flow Forecasting with Genetic Algorithm and SWMM, *Journal of Hydraulic Engineering, ASCE*, **121**(8): 613–617

Mohan, S. 1997 Parameter Estimation of Nonlinear Muskingum Models using Genetic Algorithm, *Journal of Hydraulic Engineering, ASCE*, **123**(2): 137–142

Sakanoue, T. 1969 Studies on the Precipitation of the Mountain, *Science Bulletin of the Faculty of Agriculture Kyushu University*, **24**: 29–131 (in Japanese with English summary)

Sherman, C. A. 1978 A Mass–Consistent for Wind Fields over Complex Terrain, *Journal of Applied Meteorology*, **17**: 312–319

Wakimizu, k., S. Hayashi and Y. Motoda 1988 Estimating the Precipitation on a Mountain Slope with a Vector Rain Gauge, *Transactions of the Japanese Society of Irrigation, Drainage and Reclamation Engineering*, **137**: 65–70 (in Japanese with English summary)

Zhang, X. and N. Shuto 1990 A Mass–consistent Model Applied to the Wind Field in the Upper Kitagami River Basin, *Proceedings of Hydraulic Engineering, JSCE*, **34**: 109–114 (in Japanese with English summary)